

Supplementary Information

Temperature and Salt controlled Tuning of Protein Clusters

Christian Beck,^{†,‡} Marco Grimaldo,[‡] Michal K. Braun,[†] Lena Bühl,[†] Olga
Matsarskaia,[‡] Niina H. Jalarvo,^{¶,§} Fajun Zhang,[†] Felix Roosen-Runge,^{*,||,⊥} Frank
Schreiber,[†] and Tilo Seydel^{*,‡}

[†]*Institut für Angewandte Physik, Universität Tübingen, Auf der Morgenstelle 10, 72076
Tübingen, Germany*

[‡]*Institut Max von Laue - Paul Langevin, 71 avenue des Martyrs, 38042 Grenoble, France*

[¶]*Jülich Centre for Neutron Science (JCNS), Forschungszentrum Jülich GmbH, D-52425
Jülich, Germany*

[§]*Chemical and Engineering Materials Division, Neutron Sciences Directorate, and JCNS
Outstation at the Spallation Neutron Source(SNS), Oak Ridge National Laboratory, P.O.
Box 2008, Oak Ridge, Tennessee 37831, United States*

^{||}*Department of Biomedical Sciences and Biofilms-Research Center for Biointerfaces
(BRCB), Malmö University, 20506 Malmö, Sweden*

[⊥]*Division of Physical Chemistry, Lund University, Naturvetarvägen 14, 22100 Lund,
Sweden*

E-mail: felix.roosen-runge@mau.se; seydel@ill.eu

q -dependence of some representative fit results describing the apparent global diffusion

The experimental data were fitted in a first approach with Equation 1-3 of the main text for each q individually. In this way, we confirm that the center-of-mass diffusion agrees with simple Brownian diffusion. The internal diffusion is described in this approach with one free Lorentzian function. Figure S1 displays the width of the narrow Lorentzian function as a function of q^2 . Deviations from the expected linearity at high q can be observed in the fits per q . These deviations can be attributed to effects of cross-talking between the different Lorentzians in these q -wise fits that do not impose any the q -dependence. This cross-talking may notably include contributions from the protein internal dynamics of the protein backbone as well as indirect effects from the de Gennes narrowing observed in the solvent line width at the position of the D₂O nearest neighbor correlation.¹

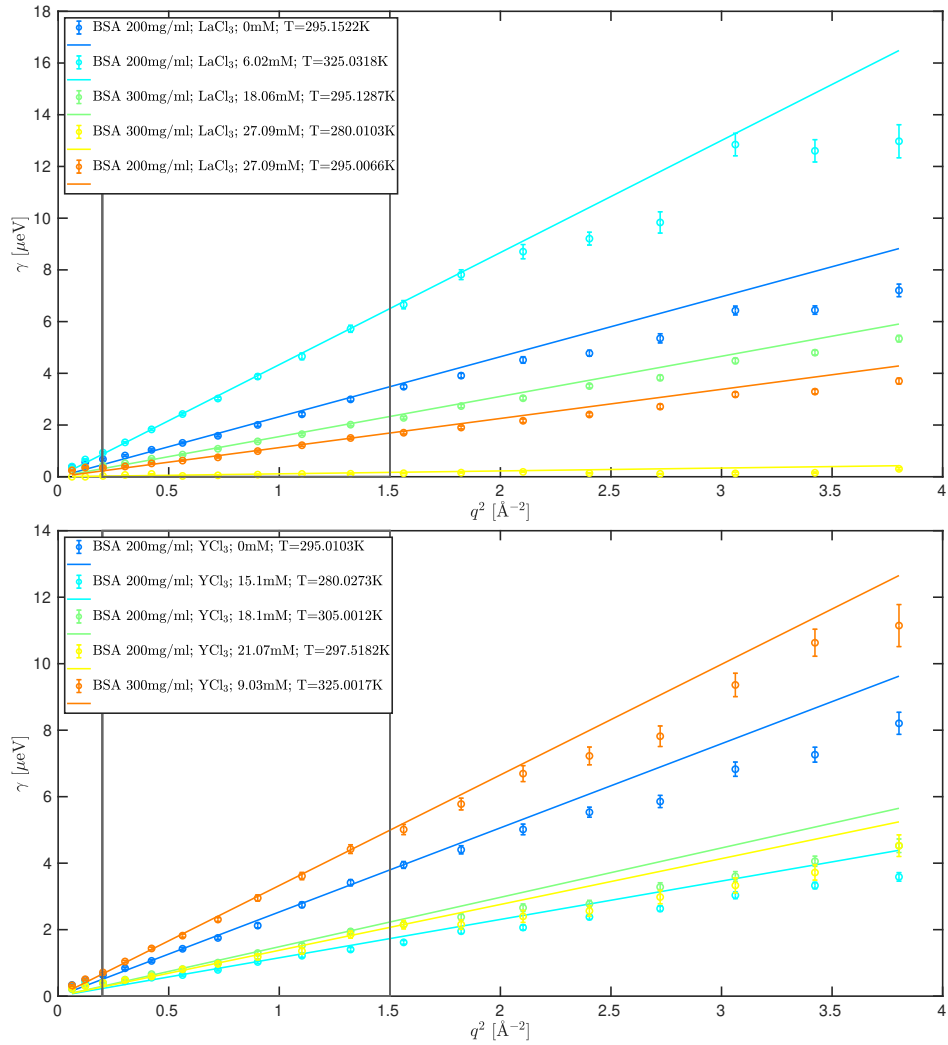


Figure S1: Representative fit results (γ) of different samples as a function of q^2 .

Model for the global fits

The experimental data were analyzed using a model which describes the global diffusion via Brownian diffusion and the internal diffusion with two linked Lorentzian functions:^{2,3}

$$S_{\text{Prot,int}} = \xi \mathcal{L}_{\lambda_1}(\omega) + (1 - \xi) \mathcal{L}_{\lambda_2}(\omega) \quad (1a)$$

$$\xi = \frac{\tau_1 \Gamma_2 + \tau_2 \Gamma_1 + (\tau_1 + \tau_2)(\tau_1^{-1} + \tau_2^{-1} - \lambda_1)}{(\lambda_2 - \lambda_1)(\tau_1 + \tau_2)} \quad (1b)$$

$$\lambda_{1,2} = \frac{(\Gamma_1 + \tau_1^{-1}) + (\Gamma_2 + \tau_2^{-1}) \pm \Lambda}{2} \quad (1c)$$

$$\Lambda = \sqrt{[(\Gamma_1 + \tau_1^{-1}) - (\Gamma_2 + \tau_2^{-1})]^2 + \frac{4}{\tau_1 \tau_2}} \quad (1d)$$

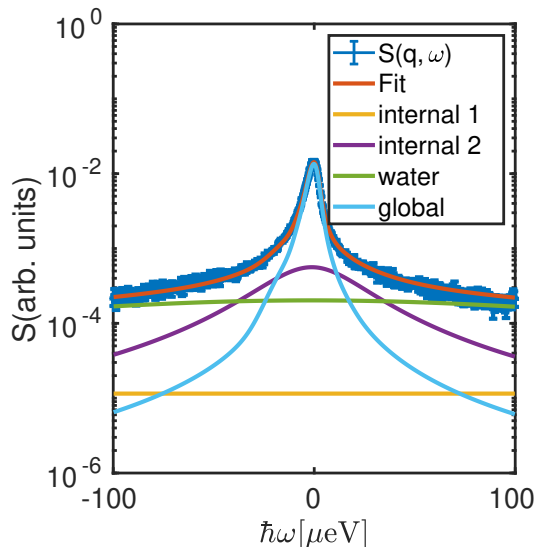
$$\Gamma_{1,2} = D_{1,2} q^2 \quad (1e)$$

Importantly, only $D_{1,2}$ and $\tau_{1,2}$ are fit parameters. By performing a global fit describing the energy and momentum transfer, the number of fit parameters is reduced as indicated in Table 1 and more complex models can be fitted. By considering only three different q values within the fit, fewer parameters are needed and render the fit more robust. We used all available momentum transfers ($0.2 \text{ \AA}^{-1} < q < 1.5 \text{ \AA}^{-1}$).

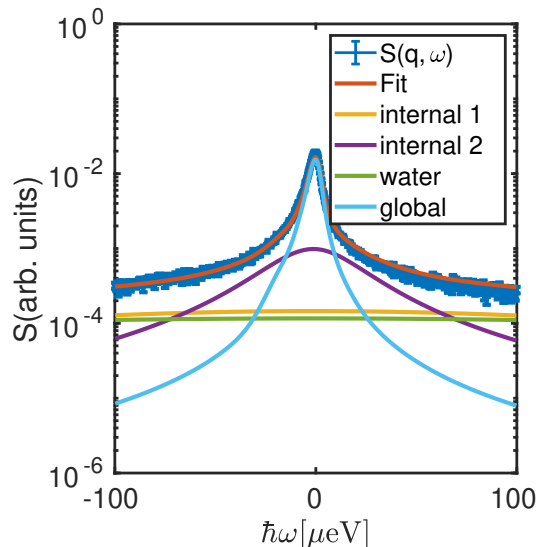
Table 1: Numbers of fit parameters for different fit models considering a total number of n momentum transfers q :

Parameter	Two free Lorentzian Functions	Global fit model as described in Equation 1
β	n	n
A_0	n	n
global diffusion	n	1
internal diffusion	n	4
total number of fit parameters	$4 \cdot n$	$2 \cdot n + 5$

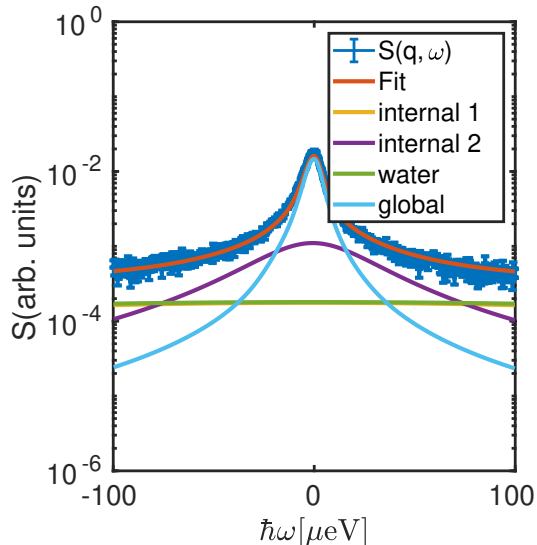
Example fits



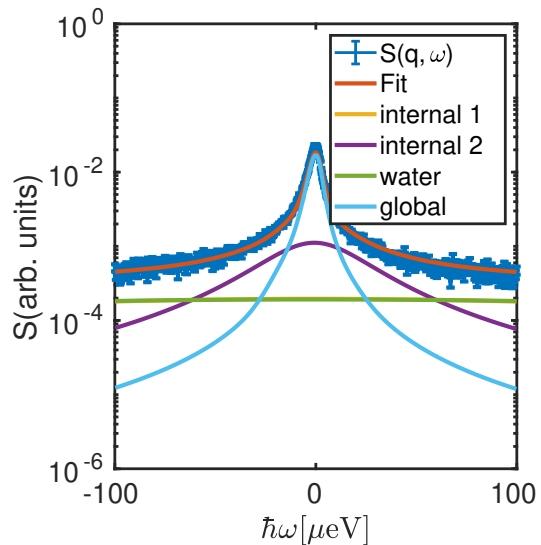
(a) BSA $c_p = 200 \frac{\text{mg}}{\text{ml}}$; LaCl_3 ; $c_s = 21.07 \text{ mM}$; $T = 295 \text{ K}$; $q = 1.0 \text{ \AA}^{-1}$.



(b) BSA $c_p = 300 \frac{\text{mg}}{\text{ml}}$; LaCl_3 ; $c_s = 36.12 \text{ mM}$; $T = 325 \text{ K}$; $q = 1.0 \text{ \AA}^{-1}$.



(c) BSA $c_p = 300 \frac{\text{mg}}{\text{ml}}$; YCl_3 ; $c_s = 9.03 \text{ mM}$; $T = 325 \text{ K}$; $q = 1.0 \text{ \AA}^{-1}$.



(d) BSA $c_p = 200 \frac{\text{mg}}{\text{ml}}$; YCl_3 ; $c_s = 18.1 \text{ mM}$; $T = 325 \text{ K}$; $q = 1.0 \text{ \AA}^{-1}$.

Figure S2: Quasi-elastic neutron backscattering spectra $S(q, \omega)$ measured at BASIS during experiments IPTS 15974.1 and 18578.1. The example spectra of different samples illustrate the results of the global fits (*i.e.*, for all q simultaneously) using Equation 1 to describe the internal motions of the protein.

Internal diffusion

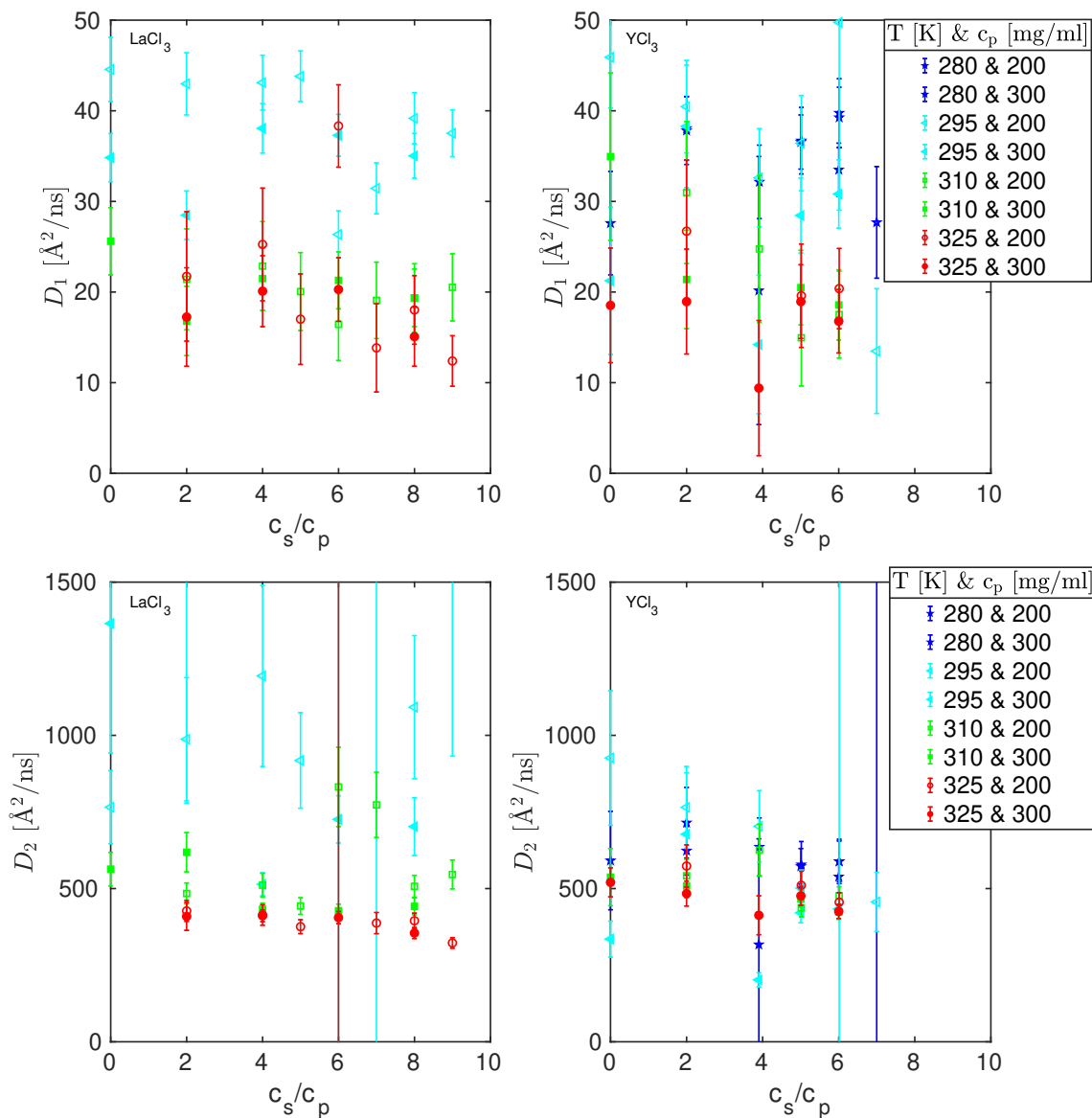


Figure S3: Diffusion coefficients obtained based on the switching model (Equation 1) describing the internal protein dynamics as a function of salt cations per protein for different temperatures. Open and filled symbols represent samples with 200 mg/ml and 300mg/ml BSA, respectively.

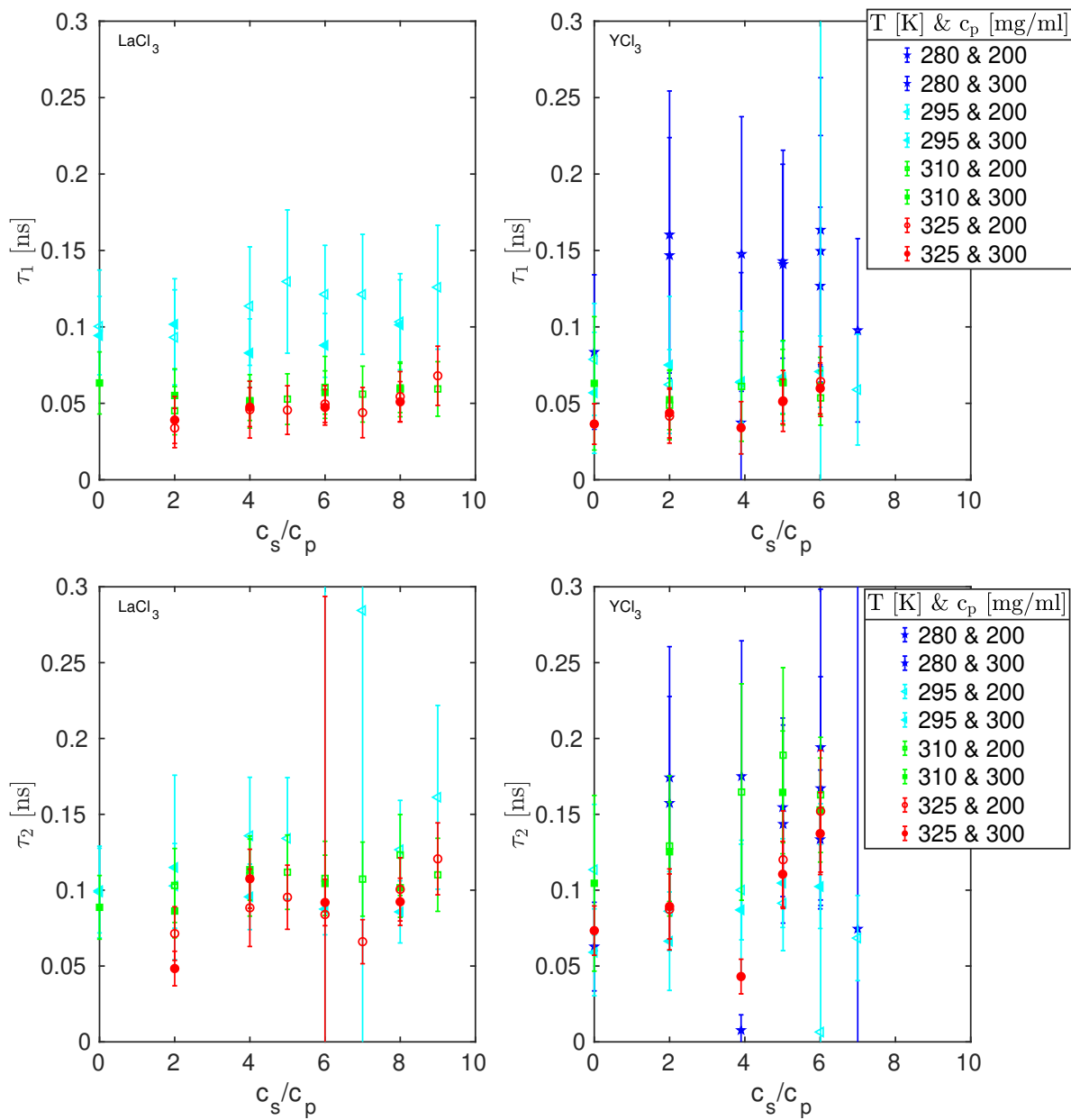


Figure S4: Residence times based on the switching model (Equation 1) describing the internal protein dynamics as a function of the number of salt cations per protein for different temperatures. Open and filled symbols represent samples with 200 mg/ml and 300mg/ml BSA, respectively.

Comparison of the parametrization with previous experiments

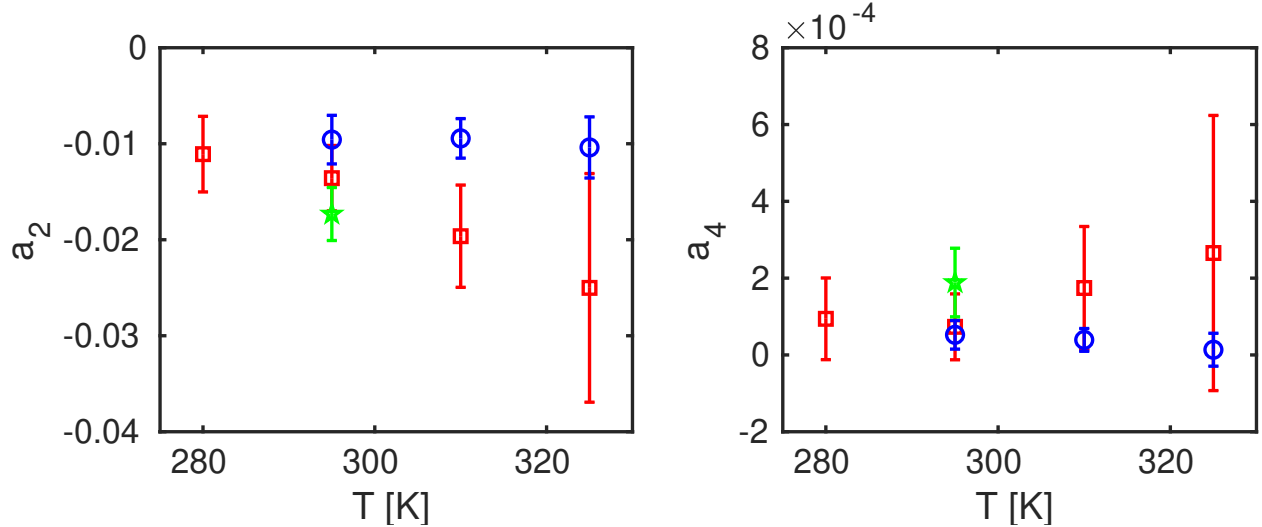


Figure S5: Fit results of Equation 16 of the main article parametrizing the master curves for the different temperatures and salts. Different temperature dependencies are visible for the different salts. Blue circles, red squares and green stars represent the temperature-dependent data from samples with LaCl₃ and YCl₃, as well as the results obtained by Grimaldo *et al.*⁴ for BSA and YCl₃ at 295 K, respectively.

Stickiness parameter

Based on the normalized diffusion coefficients shown in Figure 2 of the main text, the stickiness parameter τ_S was extracted:⁵

$$D = D^{dil}(1 - \lambda_A \phi) \quad (2)$$

$$\lambda_A = -1.8315 - \left(\frac{0.295}{\tau_S} \right) \quad (3)$$

$$\frac{D}{D_0} \stackrel{(1)}{=} 1 - \frac{0.295\phi}{\tau_S(1 - 1.8315\phi)} \quad (4)$$

with D^{Dil} being the diffusion coefficient in the dilute limit. At (1), it was assumed, that in the absence of salt, $\tau_S \rightarrow \infty$.

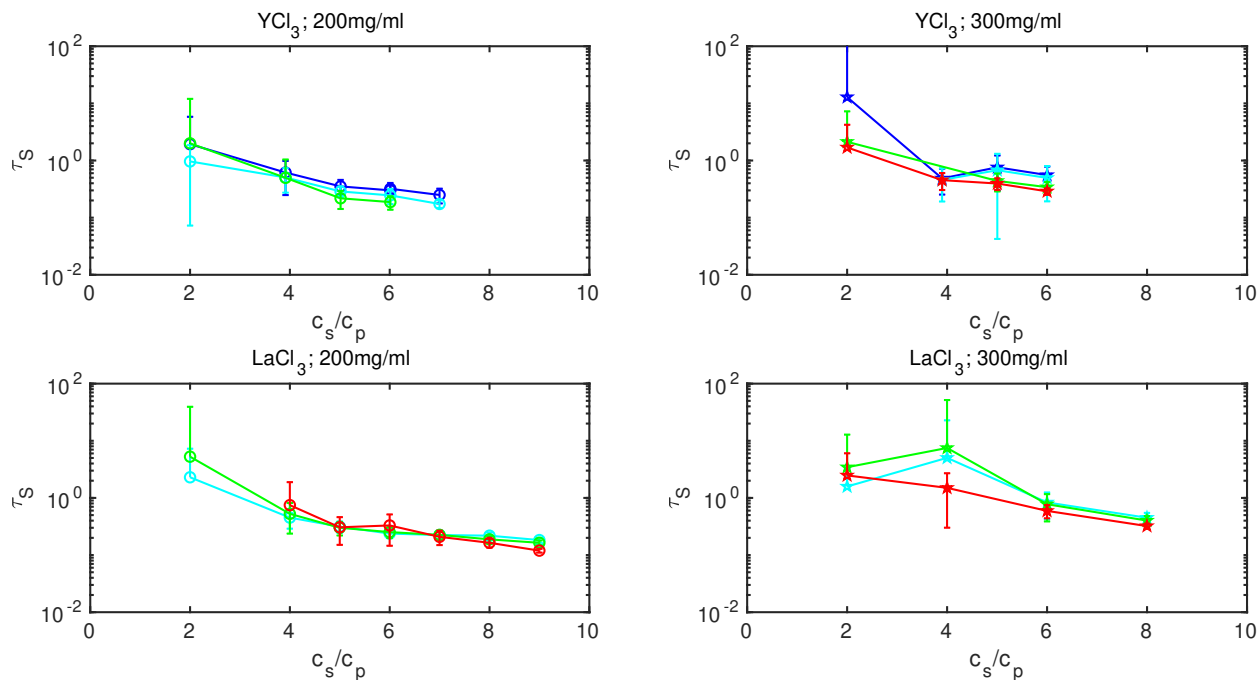


Figure S6: Stickiness parameter as a function of c_s/c_p calculated based on Equation 4 for the salts and different temperatures investigated. Blue, cyan, green and red symbols represent measurements at $T = 280$ K, 295 K, 310 K, 325 K, respectively.

Theoretical center-of-mass diffusion coefficients

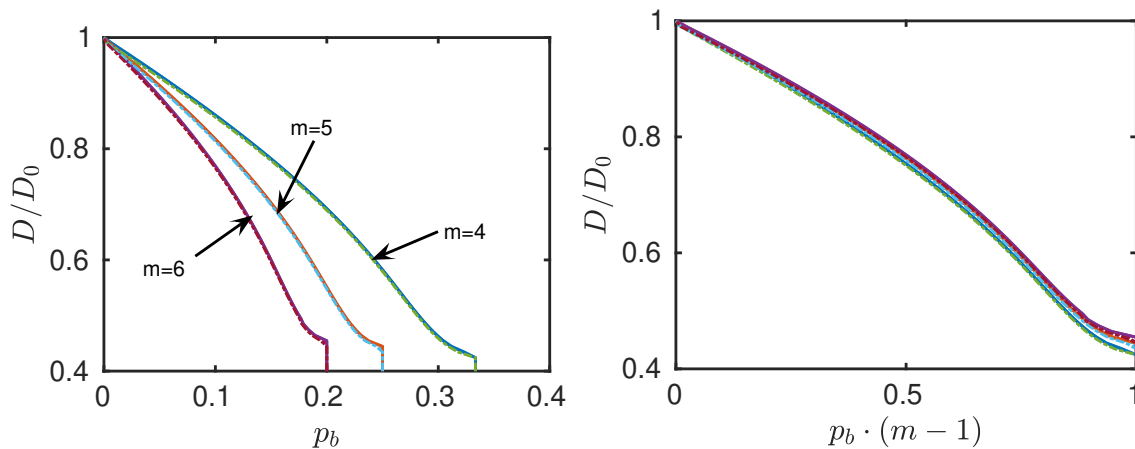


Figure S7: Left: Normalized diffusion coefficients as a function of the binding probability p_b (based on Equation 10 in the main text). Different calibration curves are shown for different m values as indicated. Solid and dashed lines represent calibration curves for $T = 280$ K and $T = 325$ K, respectively.

Right: Normalized diffusion coefficients as a function of $p_b \cdot (m - 1)$. The color code is the same as in the left subplot. Only a small difference in the dependence on m is visible.

Binding probabilities p_b and protein-protein attraction strength $\varepsilon_{AB}(T = 20^\circ\text{C})$ for different numbers of binding sites m

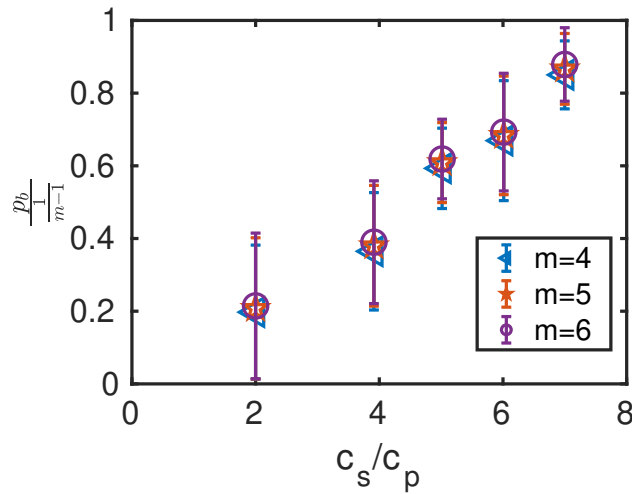


Figure S8: Binding probabilities p_b as a function of salt ions per protein for different assumed binding sites m . The displayed binding probabilities were determined from the samples containing YCl_3 which were measured at 295K with a protein concentration of $c_p = 200 \frac{\text{mg}}{\text{ml}}$.

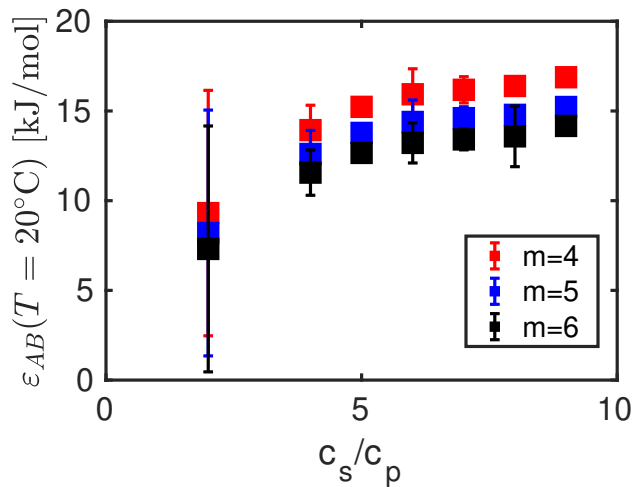


Figure S9: Protein-protein attraction strength $\varepsilon_{AB}(T = 20^\circ\text{C})$ as a function of salt ions per protein for different assumed binding sites m . The displayed values were determined from the samples containing LaCl_3 which were measured at 295K with a protein concentration of $c_p = 200 \frac{\text{mg}}{\text{ml}}$.

Small Angle Neutron Scattering Data

Small angle neutron scattering measurements were performed at D33, ILL, Grenoble, during experiment TEST-3060.⁶ The same sample preparation protocol as in the main text was used. The colored data represent the measurements of a protein solution with $c_p = 200 \frac{\text{mg}}{\text{ml}}$. The corresponding salt concentration is given by the color bar in the bottom. The left and right subplot represent mixtures with YCl_3 and LaCl_3 , respectively.

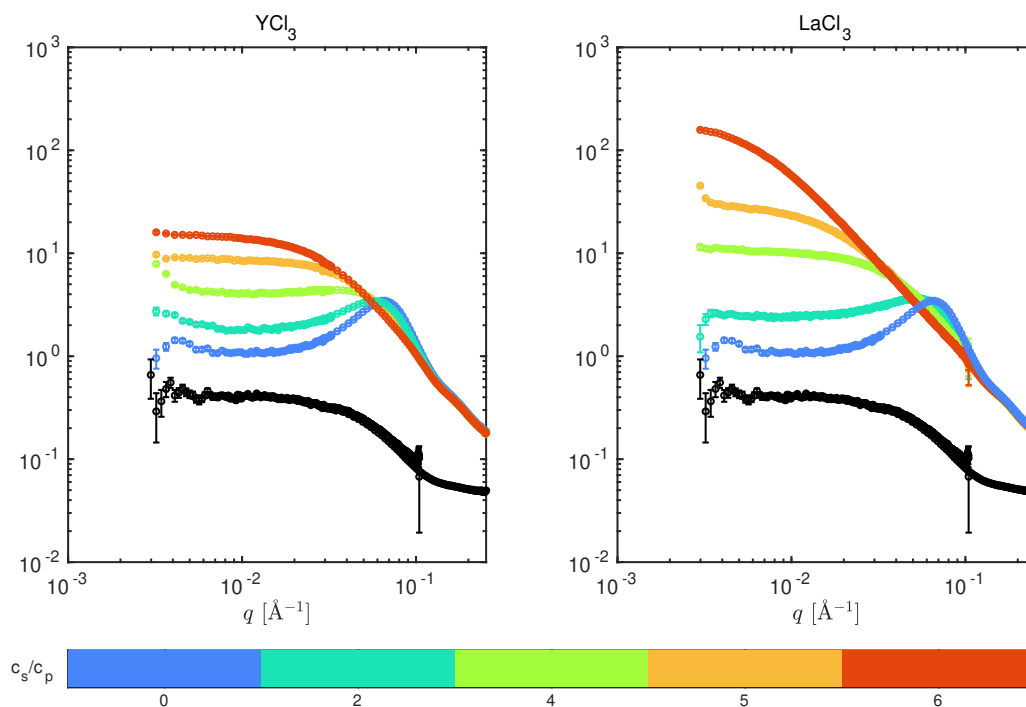


Figure S10: SANS profiles for different salt concentrations. Colored curves represent samples with a protein concentration of $c_p = 200 \frac{\text{mg}}{\text{ml}}$. The color represents the c_s/c_p value as indicated in the color bar. The black curves represent the measured form factor of a dilute BSA solution ($c_p = 5 \frac{\text{mg}}{\text{ml}}$) with NaCl (150 mM). A clear change from a system dominated by a screened Coulomb potential to an attractive system can be observed with increasing salt concentration.

References

- (1) Grimaldo, M.; Roosen-Runge, F.; Jalarvo, N.; Zamponi, M.; Zanini, F.; Hennig, M.; Zhang, F.; Schreiber, F.; Seydel, T. High-Resolution Neutron Spectroscopy on Protein Solution Samples. *EPJ Web Conf.* **2015**, *83*, 02005.
- (2) Grimaldo, M.; Roosen-Runge, F.; Hennig, M.; Zanini, F.; Zhang, F.; Jalarvo, N.; Zamponi, M.; Schreiber, F.; Seydel, T. Hierarchical Molecular Dynamics of Bovine Serum Albumin in Concentrated Aqueous Solution Below and Above Thermal Denaturation. *Phys. Chem. Chem. Phys.* **2015**, *17*, 4645–4655.
- (3) Roosen-Runge, F.; Bicout, D.; Barrat, J.-L. Analytical Correlation Functions for Motion through Diffusivity Landscapes. *J. Chem. Phys.* **2016**, *144*, 204109.
- (4) Grimaldo, M.; Roosen-Runge, F.; Hennig, M.; Zanini, F.; Zhang, F.; Zamponi, M.; Jalarvo, N.; Schreiber, F.; Seydel, T. Salt-Induced Universal Slowing Down of the Short-Time Self-Diffusion of a Globular Protein in Aqueous Solution. *J. Phys. Chem. Lett.* **2015**, *6*, 2577–2582.
- (5) Cichocki, B.; Felderhof, B. U. Diffusion coefficients and effective viscosity of suspensions of sticky hard spheres with hydrodynamic interactions. *The Journal of Chemical Physics* **1990**, *93*, 4427–4432.
- (6) Beck, C.; Cubitt, R.; Prevost, S. Following LLPS formation with SANS by temperature changes. Institut Laue-Langevin (ILL) doi:10.5291/ILL-DATA.TEST-3060. 2019.